ENVIRONMENTAL RESEARCH
LETTERS

LETTER • OPEN ACCESS

Hysteresis of the Earth system under positive and negative CO_2 emissions

Environmental Research Letters

LETTER

Hysteresis of the Earth system under positive and negative CO_2 emissions

Aurich Jeltsch-Thömmes*, Thomas F Stocker and Fortunat Joos

Climate and Environmental Physics, Physics Institute and Oeschger Centre for Climate Change Research, University of Bern, Bern, Switzerland

* Author to whom any correspondence should be addressed.

E-mail: aurich.jeltsch-thoemmes@climate.unibe.ch

Keywords: carbon dioxide removal, positive and negative emissions, hysteresis of the Earth system, carbon cycle, climate modeling

OPEN ACCESS

RECEIVED
3 June 2020

REVISED
22 September 2020

ACCEPTED FOR PUBLICATION
26 October 2020

PUBLISHED
3 December 2020

Abstract

Carbon dioxide removal (CDR) from the atmosphere is part of all emission scenarios of the IPCC that limit global warming to below 1.5 °C. Here, we investigate hysteresis characteristics in 4× pre-industrial atmospheric CO_2 concentration scenarios with exponentially increasing and decreasing CO_2 using the Bern3D-LPX Earth system model of intermediate complexity. The equilibrium climate sensitivity (ECS) and the rate of CDR are systematically varied. Hysteresis is quantified as the difference in a variable between the up and down pathway at identical cumulative carbon emissions. Typically, hysteresis increases non-linearly with increasing ECS, while its dependency on the CDR rate varies across variables. Large hysteresis is found for global surface air temperature (ΔSAT), upper ocean heat content, ocean deoxygenation, and acidification. We find distinct spatial patterns of hysteresis: ΔSAT exhibits strong polar amplification, hysteresis in O_2 is both positive and negative depending on the interplay between changes in remineralization of organic matter and ventilation. Due to hysteresis, sustained negative emissions are required to return to and keep a CO_2 and warming target, particularly for high climate sensitivities and the large overshoot scenario considered here. Our results suggest, that not emitting carbon in the first place is preferable over carbon dioxide removal, even if technologies would exist to efficiently remove CO_2 from the atmosphere and store it away safely.

1. Introduction

The future trajectory in human-caused carbon dioxide (CO_2) emissions and, therefore, global warming, is uncertain. Failure to mitigate and phase out CO_2 emissions in the last decades and the near future may cause dangerous anthropogenic climate interference (Siegenthaler and Oeschger 1978). Net negative emission scenarios were already considered in the 1990s by the Intergovernmental Panel on Climate Change (Enting *et al* 1994, Schimel *et al* 1997) and are implied in scenarios limiting global warming to below 1.5 °C (IPCC 2018). It thus remains important to investigate how climate and environmental parameters change in response to CO_2 emissions followed by CDR.

Hysteresis is the dependence of the state of a system on its history. In the Earth system, it is caused by system time lags and non-linear processes (Stocker 2000, Boucher *et al* 2012). Irreversibility arises when a perturbation in climate or the environment does not return to its unperturbed state within a time frame relevant for humans. Decadal-to-millennial timescales govern the uptake of excess carbon and heat by the ocean and by soils leading to both hysteresis and irreversibility. A range of different forcing scenarios and models has been applied to investigate hysteresis and irreversibility in Earth system responses (Maier-Reimer and Hasselmann 1987, Enting *et al* 1994, Stocker and Schmittner 1997, Plattner *et al* 2008, Lowe *et al* 2009, Samanta *et al* 2010, Frölicher and Joos 2010, Boucher *et al* 2012, Joos *et al* 2013, Tokarska and Zickfeld 2015, Zickfeld *et al* 2016, Jones *et al* 2016, Tokarska *et al* 2020).

Boucher *et al* (2012) investigate a broad range of variables in CDR scenarios, with maximum CO_2 varying between 1.5 and 4 times above preindustrial. Atmospheric CO_2 is increasing by 1% per year and decreasing at the same rate until preindustrial CO_2

in these scenarios. They found hysteresis behavior within their Earth System Model for most variables, with particularly large hysteresis in land and ocean carbon inventories, ocean heat content, and sea-level rise. Scenarios with a high maximum CO_2 concentration show larger hysteresis than those with a lower maximum. These findings are confirmed by more recent studies (MacDougall 2013, Tokarska and Zickfeld 2015, Zickfeld *et al* 2016).

Ocean warming, acidification, and deoxygenation pose serious risks to marine life (Pörtner *et al* 2014). Related impact-relevant parameters show large irreversibility and hysteresis (Mathesius *et al* 2015, Battaglia and Joos 2018). Water temperature and dissolved oxygen (O_2) are important for metabolic processes, while the pH or the saturation state of water with respect to $CaCO_3$ in the mineral form of aragonite, Ω_{arag}, are indicators of ocean acidification (Orr *et al* 2005, Gattuso and Hansson 2011). Many marine organisms, including algae and fish, build shells and other structures made of $CaCO_3$. Water is corrosive to aragonite if undersaturated ($\Omega_{arag} < 1$), and warm water corals preferentially dwell in highly supersaturated waters ($\Omega_{arag} \geq 3$), which are only found in near surface waters.

A consequence of hysteresis is that the change in surface air temperature (SAT) per trillion ton of carbon emissions, TCRE (Allen *et al* 2009, Zickfeld *et al* 2009, Matthews *et al* 2009, Steinacher *et al* 2013, Goodwin *et al* 2015, MacDougall and Friedlingstein 2015, Steinacher and Joos 2016, Williams *et al* 2016, Zickfeld *et al* 2016, Tokarska *et al* 2019), or the transient response to CO_2 emissions of any variable X per trillion ton of carbon emissions, TRE^X (Steinacher and Joos 2016), may depend on the emission path. It is found that hysteresis in SAT is small and path-dependency of TCRE weak for cumulative emissions of up to order 1 000 GtC (Zickfeld *et al* 2016) and for scenarios with a modest overshoot in emissions (Tokarska *et al* 2019), but substantial for large cumulative emissions (MacDougall *et al* 2015). Similarly, large non-linear path-dependency of TRE^X is found for steric sea level rise, the maximum strength of the Atlantic meridional overturning circulation (AMOC), Ω_{arag}, and soil carbon (Steinacher and Joos 2016).

In this study, we follow the idealized scenario approach (Samanta *et al* 2010, Boucher *et al* 2012, Zickfeld *et al* 2016) and increase atmospheric CO_2 with a rate of $1\,\%\,yr^{-1}$ followed by CDR to investigate hysteresis of the Earth system. We put aside all questions about feasibility, scalability, permanency, and direct costs or negative consequences of applying CDR technologies on global scales (Smith *et al* 2016, Fuss *et al* 2018). The focus is on scenarios with a high overshoot with peak atmospheric CO_2 reaching $4\times$ preindustrial. This corresponds to the tier 1 scenario of the CDR Model Intercomparison Project (Keller *et al* 2018). As novel elements in comparison to earlier studies, we systematically vary the rate of CDR and the climate sensitivity. We probe physical, biogeochemical, and impact-relevant variables and analyze jointly anthropogenic carbon emissions, changes (Δ) in marine and terrestrial carbon uptake and release, ΔSAT, ocean heat content (ΔOHC), ΔAMOC, the remaining sea ice area, thermocline oxygen (ΔO_2), and the volume of water with Ω_{arag} larger than 3. Finally, we present spatial patterns of hysteresis for a range of variables.

2. Methods

2.1. Model description

We use the Bern3D v2.0 s coupled to the LPX-Bern v1.4 dynamic global vegetation model. The Bern3D model includes a single layer energy-moisture balance atmosphere with a thermodynamic sea-ice component Ritz *et al* (2011), a 3D geostrophic-frictional balance ocean (Edwards *et al* 1998, Müller *et al* 2006) with an isopycnal diffusion scheme and Gent-McWilliams parameterization for eddy-induced transport (Griffies 1998), and a 10-layer ocean sediment module (Heinze *et al* 1999, Tschumi *et al* 2011, Jeltsch-Thömmes *et al* 2019). The horizontal resolution across Bern3D model components is 41 × 40 grid cells and 32 logarithmically spaced depth layers in the ocean. Wind stress is prescribed from the NCEP/NCAR monthly wind stress climatology (Kalnay *et al* 1996), and gas exchange at the ocean surface and calculation of carbonate chemistry follow OCMIP-2 protocols (Najjar and Orr 1999, Wanninkhof 2014, Orr and Epitalon 2015), with an adjusted gas transfer dependency on wind speed (Müller *et al* 2008). Marine productivity is restricted to the euphotic zone (75 m) and calculated as a function of light availability, temperature, and nutrient concentrations (P, Fe, Si) (see e.g. Parekh *et al* 2008, Tschumi *et al* 2011).

In the sediment, the transport, redissolution/remineralization, and bioturbation of solid material, the pore water chemistry, and diffusion are dynamically calculated in the top 10 cm (see Tschumi *et al* 2011, for more details). Burial (loss) of nutrients, carbon, and alkalinity from the sediment is balanced by a variable input flux to the coastal surface ocean during spin-up. These weathering input fluxes are set equal to burial fluxes at the end of the spin-up for transient simulations. The Bern3D model components have been evaluated comprehensively in several studies (e.g. Roth *et al* 2014, Battaglia *et al* 2016, Jeltsch-Thömmes *et al* 2019).

The Land surface Processes and eXchanges (LPX) model v1.4 (Lienert and Joos 2018) is a further development of the Lund-Potsdam-Jena model (Sitch *et al* 2003) and simulates the coupled nitrogen, water, and carbon cycles. Here, a resolution of 2.5° latitude × 3.75° longitude is applied. Vegetation is represented by plant functional types that compete within their

bioclimatic limits for resources. A pattern scaling approach is used to pass climate information from the Bern3D on to LPX (Stocker *et al* 2013a). Spatial anomaly patterns in monthly temperature and precipitation, derived from a 21st century simulation with the Community Climate System Model (CCSM4), are scaled by the anomaly in global monthly mean surface air temperature as computed interactively by the Bern3D. These anomaly fields are added to the monthly baseline (1901 to 1931 CE) climatology of the Climate Research Unit (CRU) (Harris *et al* 2014). For further details on LPX-Bern the reader is referred to the literature (e.g. Keller *et al* 2017, Lienert and Joos 2018).

2.2. Experimental setup and analysis

The Bern3D model is spun up under 1850 CE boundary conditions with constant CO_2 of 284.7 ppm for a total of 60 000 years. Similarly, LPX-Bern is spun up under 1850 CE boundary conditions with fixed land use for 1500 years, with an acceleration step towards equilibrium for soil pools, before the models are coupled and equilibrated for another 500 years. Simulations are started from 1850 CE conditions and run for 5 000 years, while all forcing except CO_2 is kept constant. Following the protocol of the carbon dioxide removal (CDR) experiment of the CDR model intercomparison project (Keller *et al* 2018), atmospheric CO_2 is increased at a rate of 1 %yr^{-1} until 4 × CO_2 (simulation year 140). From there, prescribed CO_2 concentrations decrease at the following rates back to 284.7 ppm: 0.1, 0.3, 0.5, 0.7, 1.0, 2.0, 4.0, and 6.0 %yr^{-1} (figure 1(a)). CO_2 is kept constant thereafter. Any remaining carbon flux from the ocean and land into the atmosphere are assumed to be removed by the sustained application of negative emission technologies. All simulations are conducted with three different model setups with equilibrium climate sensitivities (ECS) of 2 °C, 3 °C, and 5 °C. The ECS are diagnosed after 5000 years in instantaneous CO_2 doubling experiments. For each setup a control run with constant atmospheric CO_2 of 284.7 ppm is included.

Cumulative carbon emissions to the atmosphere (figure 1(b)) are calculated for any period by summing the prescribed changes in the atmospheric carbon inventory (conversion: 2.12 GtC ppm^{-1}; figure 1(a), left axis) and the simulated changes in the cumulative atmosphere-ocean (figure 1(c)) and atmosphere-land biosphere (figure 1(d)) carbon fluxes.

3. Results

3.1. Carbon cycle responses

We first illustrate changes in the global carbon cycle budget (figure 1). Diagnosed cumulative emissions depend on ECS and the CDR rate. Generally, cumulative emissions are higher for low ECS than for high ECS and are in the range of 2 640 (ECS = 5 °C) to 2 885 GtC (ECS = 2 °C) in year 140 (figure 1(b)) when atmospheric CO_2 peaks at 4 × preindustrial (figure 1(a)). Cumulative emissions start to decline for all ECS with the onset of carbon dioxide removal (CDR), except for very slow CDR rates.

Anthropogenic carbon is redistributed in the Earth system (figure 1). The carbon uptake or release by the ocean depends on the difference in CO_2 partial pressure in the ocean and atmosphere, $\Delta pCO_2 = pCO_{2,ocean} - pCO_{2,atm}$ (McKinley *et al* 2020) and is governed by surface-to-deep mixing.. The ocean is the dominant net carbon sink. At peak CO_2 (year 140), 1 805 GtC have entered the atmosphere, 645 GtC the ocean, and 355 GtC the land biosphere for an ECS of 3 °C. The ocean continues to take up CO_2 for a few more centuries under slow CDR rates, as equilibrium is not yet reached due to the slow ocean overturning. For a CDR rate of 0.1 %yr^{-1}, for example, the oceanic sink peaks at 1 260 GtC (ECS = 5 °C) to 1 420 GtC (ECS = 2 °C) around simulation year 780.

The ocean turns from a sink to a source during CDR because CO_2 is removed from the atmosphere and ΔpCO_2 becomes positive. In turn, the cumulative atmosphere-ocean C flux begins to decrease. The timing and magnitude of the sign change depends primarily on the CDR rate. The faster the CDR, the earlier the ocean turns from a sink into a source. In all cases, the ocean releases carbon to the atmosphere for centuries to millennia after CO_2 is stabilized at preindustrial concentration (c.f. figures 1(a) and (c)). The cumulative atmosphere-ocean C flux varies slightly among ECS; a smaller oceanic sink for higher ECS follows from lower CO_2 solubility under higher temperatures and larger reductions in overturning (c.f. figures 1(c) and 2(a), (c)).

The cumulative atmosphere-land biosphere flux increases and declines largely in concert with CO_2 and SAT (figure 1(d)). CO_2 fertilization of plants stimulates carbon uptake under higher atmospheric CO_2 and respiration is enhanced under higher temperatures. The land biosphere sequesters about 250 GtC less in soils and litter (∼170 GtC), and vegetation (∼80 GtC) under high than low warming, mainly due to enhanced temperature-driven respiration (figure 1(d)). The cumulative atmosphere-land biosphere flux declines with CO_2 to approach zero for low and intermediate ECS. Under high ECS, the cumulative flux becomes temporarily negative. Thus, the land biosphere stores less carbon than at preindustrial. This highlights the risk that the land biosphere may not only loose excess 'anthropogenic' carbon, but even some of its 'natural' carbon inventory. The latter represents an irreversibility with potential long-term consequences for ecosystems and ecosystem services.

On millennial timescales, $CaCO_3$ compensation adds up to 200 GtC to the ocean. For most scenarios and by the end of the simulations, the cumulative

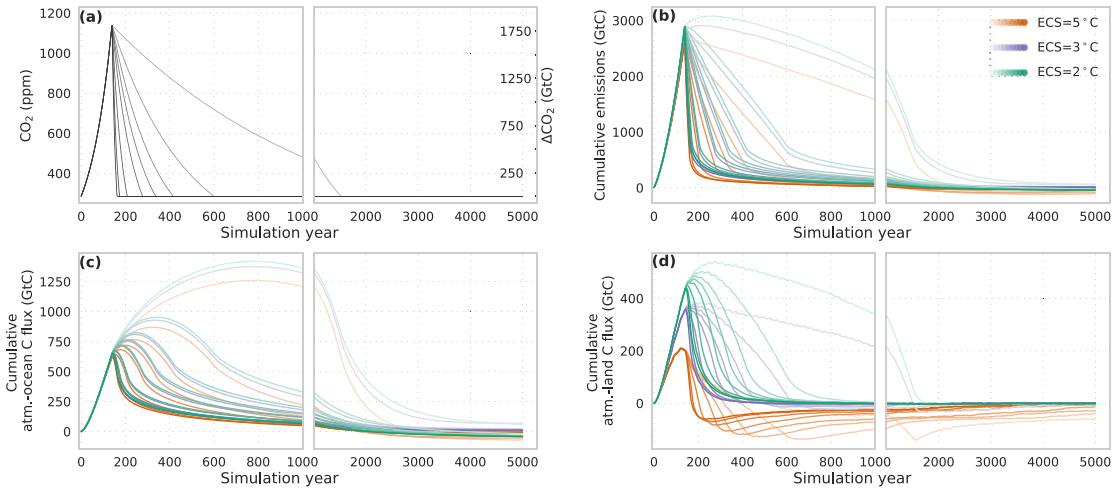

Figure 1. Timeseries of the (a) applied CO_2 forcing (left *y*-axis and grid lines) and resulting change in atmospheric carbon inventory (right *y*-axis), (b) total cumulative emissions, change in the (c) cumulative atmosphere-ocean carbon flux, and (d) cumulative atmosphere-land biosphere carbon flux. Colors indicate equilibrium climate sensitivities. The lighter the color, the lower the CDR rate. Shown is the difference to a corresponding control run.

contribution from sedimentation-weathering imbalances in the $CaCO_3$ cycle ranges between an addition of 40 GtC to a removal of 20 GtC, and no new equilibrium is reached. $CaCO_3$ compensation changes alkalinity twice as much as carbon, leading to changes in the carbon uptake capacity of the ocean, explaining the long-term perturbation in the cumulative atmosphere-ocean C flux (figure 1(c)). Imbalances in the sedimentation-weathering cycle of particulate organic carbon (POC) are small and mainly result from changes in POC preservation under lower O_2.

3.2. Physical responses

ΔSAT rises in response to higher CO_2 forcing (figure 2(a)), and at maximum cumulative emissions amounts to 2.7 °C, 3.7 °C, and 5.4 °C for ECSs of 2 °C, 3 °C, and 5 °C, respectively. The spatial warming pattern at maximum emissions resembles the global warming pattern for RCP 8.5 scenarios (IPCC 2013), with largest warming in high latitudes and over continents. Continued warming after maximum emissions scales with the subsequent removal rate and ECS. After returning to initial CO_2 concentrations, it takes centuries to millennia before SAT returns to its preindustrial value. The slower the CDR and the higher the ECS, the longer SAT stays elevated (figure 2(a)). Slow CDR scenarios and a high ECS yields ΔSAT of up to 1 °C at the end of the simulation, while for ECS = 2 °C remaining ΔSAT is below 0.1 °C.

ΔOHC is, similar to ΔSAT, largest for high ECS and slow CDR (figure 2(b)) and keeps increasing after maximum emissions. The surface ocean heat content equilibrates rather fast with the atmospheric temperature perturbation, while equilibration of the deep ocean is slow, with circulation as the rate limiting step. Thus, the slower the CDR, the longer the radiative imbalance lasts and the more of the perturbation will be transported to the deep ocean. Total OHC increases as long as the net downward heat flux at the top of the atmosphere is positive, resulting in an increase of ΔOHC by a factor >2–3 after maximum CO_2, depending on CDR (see e.g. light colors in figure 2(b)).

ΔAMOC is reduced by 4.8–8.8 Sv at maximum CO_2 forcing, depending on ECS and thus the corresponding temperature perturbation (figures 2(a) and (c)). AMOC starts to recover with declining forcing and overshoots to higher than initial values in all scenarios. The maximum overshoot is reached when CO_2 concentrations are back to initial. By the end of the simulations, AMOC states differ. Similar to SAT, slow CDR scenarios with an ECS of 5 °C show strongest deviations in AMOC strength at simulation year 5 000 and across the ensemble of runs. From the available simulations it is not clear if and when the AMOC would return to its initial strength.

Sea-ice reacts fast to changes in SAT and is substantially reduced in both hemispheres (figure 2(d)). The reduction is larger for higher ECS. Sea-ice recovers over most of the simulations. For ECS = 2 °C, however, sea-ice area seems to stabilize at ∼95% of its initial cover. The slow recovery and partial reversion into a new reduction of sea-ice area during and after CDR (see e.g. orange lines around year 600 in figure 2(d)) is driven by Southern Hemisphere (SH) sea-ice changes. Generally, the reduction in the SH is larger than in the Northern Hemisphere (NH) and longer lasting.

3.3. Hysteresis

We quantify hysteresis as the difference in a variable between the up-path with increasing cumulative

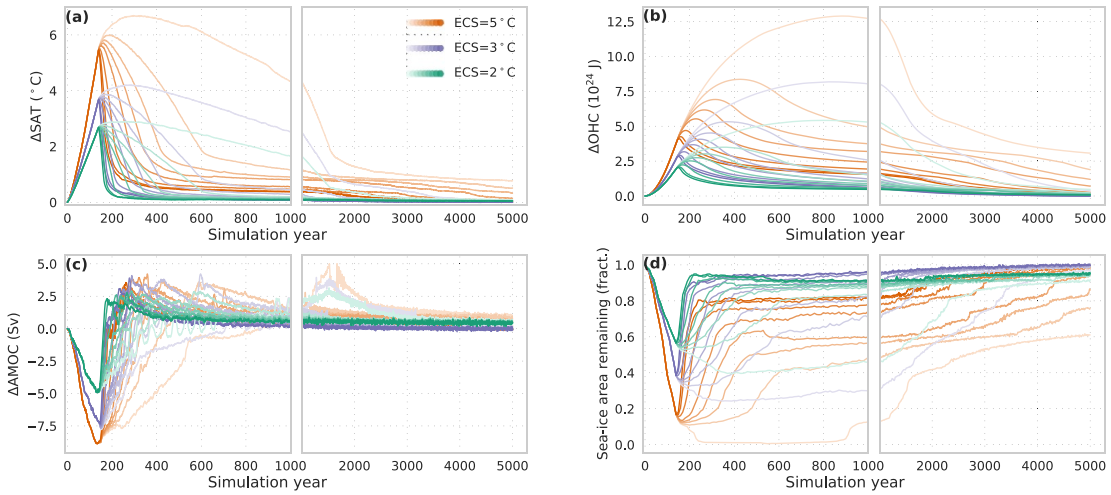

Figure 2. Timeseries of the anomalies (Δ) in the (a) global mean surface air temperature (SAT), (b) total ocean heat content (OHC), (c) maximum strength of the Atlantic meridional overturning circulation (AMOC), and (d) remaining fraction of global sea-ice area. Colors as in figure 1.

emissions and the down-path with decreasing cumulative emissions at 1000 GtC of cumulative carbon emissions. We thus consider large overshoot scenarios of up to about 2000 GtC (figure 1(b)).

We first examine differences in SAT between the up-path (dashed lines) and down-path (solid lines; figure 3(a)). Generally, the higher the ECS, the larger the hysteresis (see bars at the right of figure 3(a)). Non-linearities in SAT in the cumulative emission space do not scale linearly with ECS. For an ECS of 2 °C, hysteresis is small and largely negative. With ECS = 3 °C, SAT is in the mean 0.1 °C higher for the down- than up-path, while for ECS = 5 °C this difference increases to 1.5 °C. This means that at cumulative emissions of 1000 GtC and an ECS of 2 °C temperatures are mostly lower on the down-path compared to the up-path, while for ECS of 3 and 5 °C they are higher.

Upper ocean (700 m) heat content (OHC_{700}, figure 2(b)) shows similar hysteresis as SAT. With decreasing cumulative emissions, OHC_{700} first keeps increasing, until atmosphere and upper ocean are in equilibrium. For all three ECS, the mean hysteresis width is positive and ranges between 0.4 and 1.8 10^{24} J.

Changes in O_2 result from changes in O_2 consumption due to remineralization, from changes in O_2 solubility, and to a lesser extent from changes in air-sea disequilibrium. Remineralization-driven changes in O_2 correlate well with changes in ideal age (not shown): the weaker the ventilation and thus the older the water masses, the more oxygen is consumed by remineralization of organic matter. In many regions, ocean overturning circulation and ventilation is reducing under global warming causing O_2 to decline. Higher temperatures at the surface lead to lower O_2 solubility and lower surface concentrations which are then transported to the ocean interior. Reductions in thermocline O_2 are larger for higher than lower ECS (figure 3(c)). The mean hysteresis width for an ECS of 5 °C is about –4 mmol m^{-3}, while for ECS = 3 °C and ECS = 2 °C it is positive.

In contrast to SAT or O_2, changes in Ω_{arag} depend weakly on the ECS, but vary with the rate of CDR (figure 3(d)). Ω_{arag} decreases with increasing dissolved CO_2. Therefore, Ω_{arag} follows the increase and decline in atmospheric CO_2 without much delay in near surface waters and with delay in the deep ocean. At atmospheric CO_2 of about 565 ppm and cumulative emissions close to 1 000 GtC, there are almost no waters left with $\Omega_{arag} > 3$. The decrease in cumulative emissions is delayed relative to the decrease in atmospheric CO_2, and Ω_{arag} starts to recover at much higher cumulative emissions during the down-path relative to the up-path. This hysteresis is particularly large for low CDR rates (figure 3(d)). Recovery of Ω_{arag} is generally faster for low ECS in the cumulative emissions space, resulting from larger contributions of changes in ocean and land carbon to the emission budget (see figure 1). CDR is potentially highly effective in mitigating near surface ocean acidification quickly, but deep ocean acidification is, as the perturbation in ocean carbon (figure 1(c)), long-lived.

3.4. Spatial patterns of hysteresis

Next, we focus on the spatial patterns of hysteresis in SAT and O_2 and how they vary with ECS. We compare spatial anomalies for the CO_2 down-path minus the up-path at cumulative emissions of 1 000 GtC and a CDR rate of 1 %yr^{-1} (figure 4). 1 000 GtC are reached in simulation year 67, 68, and 69 on the up-path, and in simulation year 257, 249, and 231 on the down-path for ECS of 2 °C, 3 °C, and 5 °C, respectively. We again consider large levels of overshoot above the baseline of 1 000 GtC.

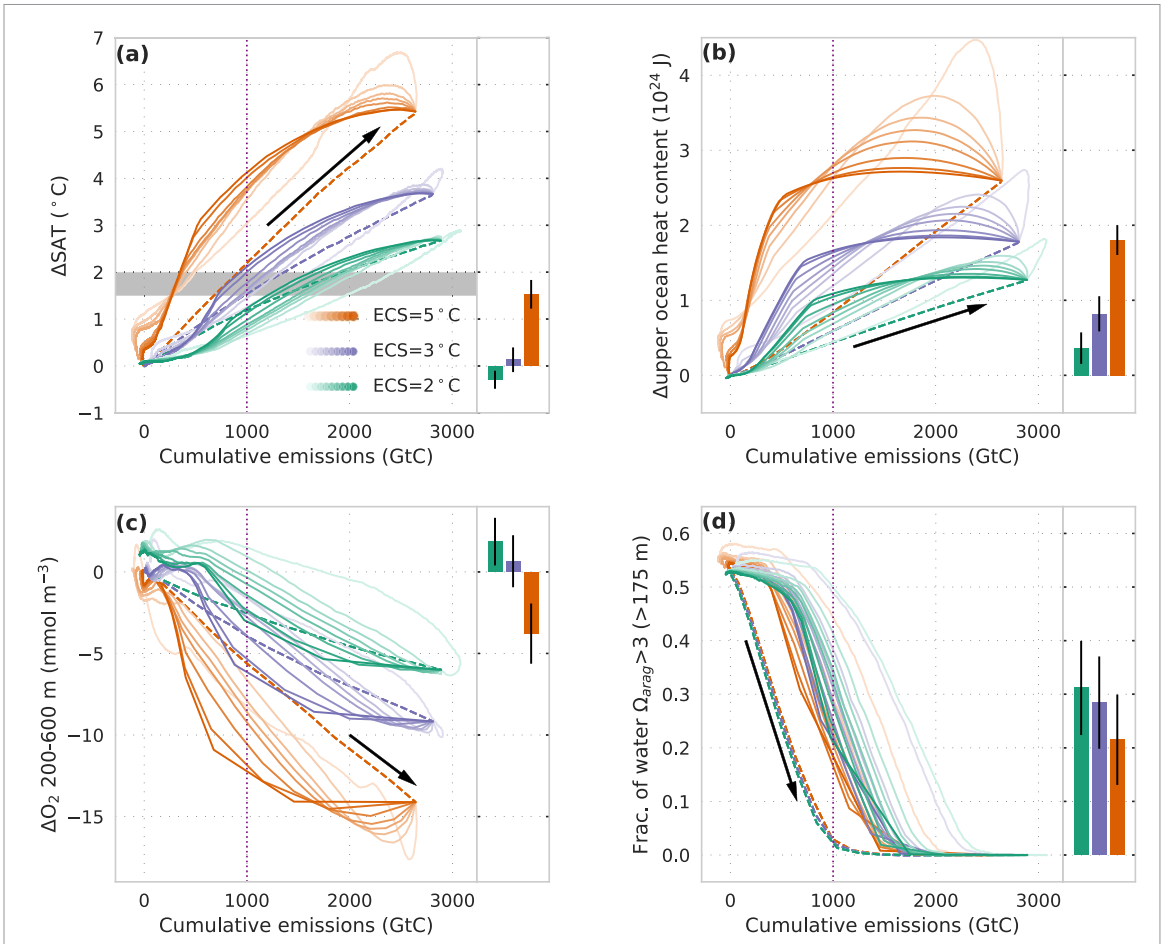

Figure 3. Hysteresis for (a) ΔSAT, (b) Δupper ocean (0–700 (m) heat content, (c) ΔO_2 in the thermocline (200 m–600 m), and (d) fraction of water with aragonite saturation state Ω_{arag} >3. Bar plots show the mean and ±1 standard deviation of the hysteresis at 1 000 GtC cumulative emissions (vertical dashed purple line) across all CDR rates for each ECS (colors). Grey shading in (a) shows the range of 1.5–2 °C warming. The upward CO_2 path is indicated by the arrows and dashed lines. It lasts 140 years, while the CO_2 decline and stabilization period (solid lines) extends over 4860 years. Colors as in figure 1.

The hysteresis of SAT is largely negative for an ECS of 2 °C and becomes positive for higher ECS (figures 3(a) and 4(a), (c) and (e)). A clear polar amplification is visible across all three ECSs. Highest positive temperature differences are located over Alaska and Eastern Siberia and in the Bering and Chukchi Seas, and in the Atlantic sector of the Southern Ocean. These regions show reduced sea-ice area and thus a lower albedo for the down-path compared to the up-path (see figure 2(d)).

Thermocline O_2 shows spatially varying positive and negative hysteresis. Hysteresis of O_2 is negative in the Arctic, the Atlantic south of the equator, and most of the Pacific. The Atlantic north of the equator and the northern Pacific show large positive hysteresis in thermocline O_2 (figures 4(b), (d) and (f)). The pattern is generally comparable between different ECSs. In parts of the North Pacific and in the Southern Ocean, however, thermocline O_2 shows positive hysteresis for ECSs of 2 °C and 3 °C, while for ECS = 5 °C the hysteresis is negative. The hysteresis patterns result from the interplay of consumption of O_2 during remineralization, ventilation of water masses, and contributions from temperature anomalies to the solubility component of oxygen, $O_{2,sol}$. Hysteresis in thermocline $O_{2,sol}$ is generally negative, except in the Southern Ocean for ECS of 2 and 3 °C with slightly positive values (not shown). The most negative $O_{2,sol}$ differences coincide with the O_2 hysteresis minima in the Arctic and the Atlantic south of the equator.

The Indian Ocean, the tropical Western and Northeastern Pacific, the Atlantic north of the equator and the Atlantic sector of the Southern Ocean show minima in ideal age hysteresis (not shown), indicating higher ventilation of waters in the thermocline. Directly around Antarctica, water mass age increases for ECS = 5 °C. On top, export production exhibits most negative hysteresis in the North Atlantic in response to a weaker AMOC and thus reduced nutrient supply, and most positive hysteresis around Antarctica as a result of reduced sea-ice cover. Together, reduced water mass age and less export production lead to less oxygen consumption (i.e. Indian Ocean, Atlantic north of the equator, parts of the Pacific), while less ventilation and increased export production as seen around Antarctica yield lower O_2 on the down-path than on the up-path for ECS of

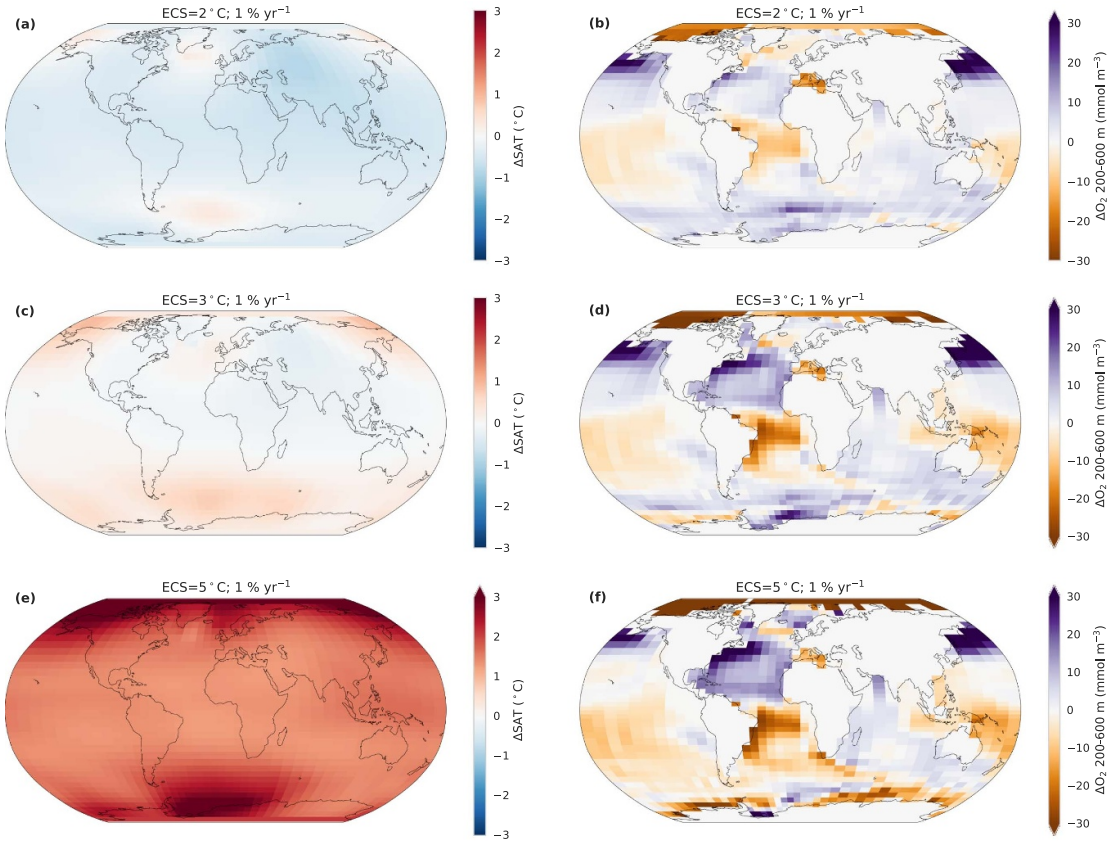

Figure 4. Hysteresis in (a), (c), (e) SAT and (b), (d), (f) thermocline O_2 (down-path minus up-path at cumulative emissions of 1 000 GtC). Results are for a decrease rate of 1 % yr^{-1} and for ECSs of (a), (b) 2 °C, (c), (d) 3 °C, and (e), (f) 5 °C.

2 °C and 3 °C (figures 4(b) and (d)). For ECS = 5 °C, and to a lesser extent ECS = 3 °C, negative hysteresis in $O_{2,sol}$ and positive hysteresis in ideal age around Antarctica lead to the sign change in O_2 hysteresis there (figures 4(d) and (f)).

Finally, in the case of Ω_{arag}, differences between the three ECS are small (figure 3(d)). Ω_{arag} is generally lower during rising CO_2 than during CDR for the same cumulative emissions (figures 3(d) and 5). The recovery is strongest in the sub-tropics, where Ω_{arag} reaches values >3 in most areas (figure 5(b)). The tropics show slightly higher Ω_{arag} values for CDR compared to emissions, while the high latitudes are similar for the two time slices (figure 5).

4. Discussion

Results from our experiments with different, highly idealized carbon dioxide removal (CDR) rates for three different equilibrium climate sensitivities (ECS) have several implications. The response in global mean surface air temperature (SAT) to positive cumulative carbon emissions is nearly linear and has been used to calculate the remaining carbon budget in order to reach certain climate targets (e.g. Matthews *et al* 2009, Steinacher *et al* 2013, IPCC 2013, Stocker 2013, Goodwin *et al* 2015, Rogelj *et al* 2019). Similarly, the proportionality between SAT (and many other variables) and atmospheric CO_2 (e.g. Armour *et al* 2011, Boucher *et al* 2012, Li *et al* 2013) and cumulative emissions (e.g. Zickfeld *et al* 2016) has been investigated for idealized CDR. In the case of SAT, for example, a non-linear response during the up- and down-path of CO_2 has been found, as in this study. With higher ECS, however, this non-linearity in the cumulative emissions space increases in the large overshoot scenarios considered here (figure 3(a)). The remaining carbon budget should, therefore, not be computed from the established relationship between positive cumulative carbon emissions and ΔSAT (Allen *et al* 2009, Stocker *et al* 2013b) for high overshoot scenarios with CDR. This non-linearity implies that in order to return to a certain temperature with the help of CDR requires the removal of more carbon than was emitted after passing the same temperature on the up-path (see also MacDougall 2013, MacDougall *et al* 2015).

Other physical and biogeochemical variables such as changes in ocean heat content, AMOC strength, or thermocline O_2 show, as SAT, increasing hysteresis with higher ECS, while for the Ω_{arag} saturation state hysteresis is smaller under high ECS. Potentially higher ECS of the Earth system than previously assessed (Forster *et al* 2020), underscores the urgency of emissions reduction to net zero (see also discussion below).

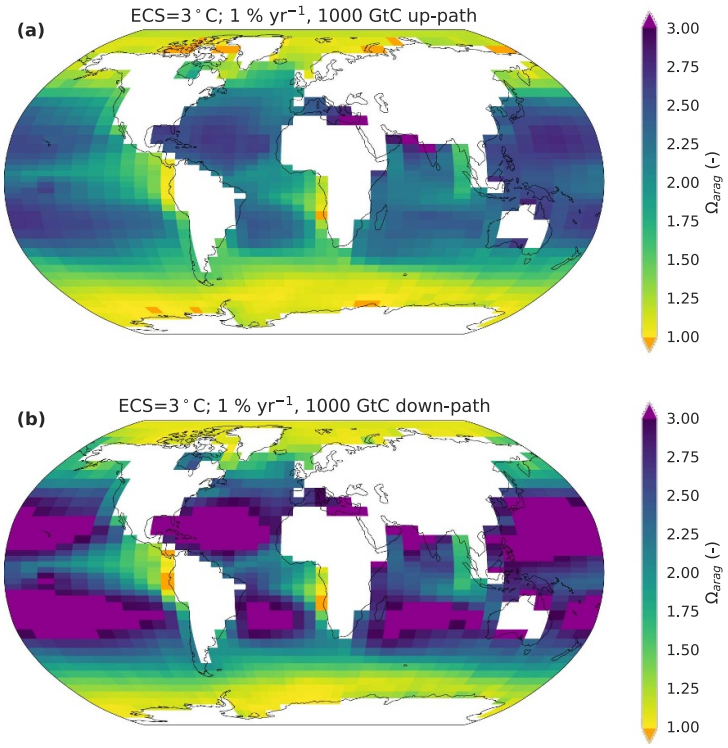

Figure 5. Mean aragonite saturation state (Ω_{arag}) of the uppermost 175 m (first four vertical layers in the model) for cumulative emissions of 1 000 GtC on the (a) up-path and (b) down-path, and an ECS of 3 °C and a CDR rate of 1 %yr^{-1}.

There are several limitations to our study. First, we use an Earth system model of intermediate complexity (EMIC). Besides the benefits, such as the possibility to cover a wide range of CDR rates for different ECSs and to run the model for several millennia, EMICs come with drawbacks. Many processes are implemented as simplified parameterizations, the atmosphere consists of an energy-moisture balance model with no atmospheric dynamics. For example, the cloud feedback is only indirectly parameterized in the Bern3D, with possible implications for the response to changes in radiative forcing (see e.g. Andrews *et al* 2015). Also, changes in continental ice-sheets are not simulated by the model but might well affect, for example, the response in AMOC. Nevertheless, the Bern3D-LPX model has been shown to perform well in comparison to observational data (e.g. Roth *et al* 2014) and comparable to other models in model intercomparison projects (Joos *et al* 2013, Eby *et al* 2013, MacDougall *et al* 2020), and has been used in several studies investigating the Earth system response to different emission scenarios (e.g. Steinacher *et al* 2013, Steinacher and Joos 2016, Pfister and Stocker 2016, Battaglia and Joos 2018).

Second, we apply highly idealized scenarios. Our maximum CO_2 forcing corresponds to a 4 × CO_2 scenario, comparable to a high emission scenario such as the Shared Socioeconomic Pathway (SSP) 5–8.5 (Riahi *et al* 2017). Future efforts might focus more on scenarios in line with the UNFCCC Paris Agreement's goal of holding global warming well below 2 °C. Previous studies show that the hysteresis in SAT varies with the amount of overshoot (Boucher *et al* 2012, Zickfeld *et al* 2016, Tokarska *et al* 2019). For small overshoots of the carbon budget of up to 300 GtC, SAT shows almost no hysteresis (Tokarska *et al* 2019), while it is larger for high overshoot scenarios (MacDougall *et al* 2015, Zickfeld *et al* 2016).

Third, concerning the chosen range of ECS, there is a large body of literature on estimates of the ECS of the Earth system. The last IPCC report concluded the ECS to lie within 1.5 to 4.5 °C with a probability of 66% (IPCC 2013). The review by Sherwood *et al* (2020) suggests for the effective climate sensitivity a 66% probability range of 2.6–3.9 °C, which remains within the bounds 2.3–4.5 °C under plausible robustness tests. This is consistent with earlier Bern3D observation-constrained estimates (2.0–4.2 °C; 68% range (Steinacher and Joos 2016)). The concept of equilibrium or effective climate sensitivity does not (or hardly) account for slowly evolving Earth System feedbacks (Heinze *et al* 2019), e.g. those associated with ice sheet albedo changes and many feedbacks involving biogeochemical cycles and GHGs. Here, we implicitly account for these additional feedbacks, beyond the carbon cycle-climate feedbacks explicitly modelled in Bern3D-LPX, by using an upper bound of 5 °C for ECS.

In summary, the response of the Earth system to positive and negative CO_2 emissions differs. This

hysteresis is sensitive to the choice of equilibrium climate sensitivity and carbon dioxide removal rate in the Bern3D-LPX model. Further, we investigate emission scenarios featuring a large level of overshoot above a chosen baseline of 1 000 GtC cumulative emissions. Generally speaking, our results suggest that no emissions is a better strategy than carbon dioxide removal, even if technologies existed to remove CO_2 from the atmosphere and store it away safely and permanently. Negative emissions are considered in scenarios with a 1.5 °C warming target (IPCC 2018) as the required rate of emissions reduction seems unrealistically fast without allowing for an overshoot in temperature and subsequent CDR.

Acknowledgments

AJT acknowledges support from the Oeschger Centre for Climate Change Research.

TFS acknowledges funding from the Swiss National Science Founation (SNF 200020_172745) and the EU Commission (H2020 project TiPES, grant 820970). This is TiPES contribution #53. FJ acknowledges funding from Swiss National Science Foundation (SNF 200020_172476) and the from the European Union's Horizon 2020 research and innovation programme under grant agreement No 820989 (project COMFORT, Our common future ocean in the Earth system—quantifying coupled cycles of carbon, oxygen, and nutrients for determining and achieving safe operating spaces with respect to tipping points). The work reflects only the authors' view; the European Commission and their executive agency are not responsible for any use that may be made of the information the work contains.

Data Availability

The data that support the findings of this study are available upon reasonable request from the authors.

ORCID iDs

Aurich Jeltsch-Thömmes https://orcid.org/0000-0002-2050-1975
Thomas F Stocker https://orcid.org/0000-0003-1245-2728
Fortunat Joos https://orcid.org/0000-0002-9483-6030

References

Allen M R, Frame D J, Huntingford C, Jones C D, Lowe J A, Meinshausen M and Meinshausen N 2009 Warming caused by cumulative carbon emissions towards the trillionth tonne *Nature* **458** 1163–6

Andrews T, Gregory J M and Webb M J 2015 The dependence of radiative forcing and feedback on evolving patterns of surface temperature change in climate models *J. Clim.* **28** 1630–48

Armour K C, Eisenman I, Blanchard-Wrigglesworth E, McCusker K E and Bitz C M 2011 The reversibility of sea ice loss in a state-of-the-art climate model *Geophys. Res. Lett.* **38** L16705

Battaglia G and Joos F 2018 Hazards of decreasing marine oxygen: the near-term and millennial-scale benefits of meeting the Paris climate targets *Earth Syst. Dyn.* **9** 797–816

Battaglia G, Steinacher M and Joos F 2016 A probabilistic assessment of calcium carbonate export and dissolution in the modern ocean *Biogeosciences* **13** 2823–48

Boucher O, Halloran P R, Burke E J, Doutriaux-Boucher M, Jones C D, Lowe J, Ringer M A, Robertson E and Wu P 2012 Reversibility in an Earth System model in response to CO_2 concentration changes *Environ. Res. Lett.* **7** 024013

Eby M *et al* 2013 Historical and idealized climate model experiments: an intercomparison of Earth system models of intermediate complexity *Climate Past* **9** 1111–40

Edwards N R, Willmott A J and Killworth P D 1998 On the role of topography and wind stress on the stability of the thermohaline circulation *J. Phys. Oceanogr.* **28** 756–78

Enting I, Wigley T, and Heimann M 1994 Future emissions and concentrations of carbon dioxide: key ocean/atmosphere/land analyses *Tech. rep.* CSIRO Division of Atmospheric Research Technical Paper no. 31

Forster P M, Maycock A C, McKenna C M and Smith C J 2020 Latest climate models confirm need for urgent mitigation *Nat. Clim. Change* **10** 7–10

Frölicher T L and Joos F 2010 Reversible and irreversible impacts of greenhouse gas emissions in multi-century projections with the NCAR global coupled carbon cycle-climate model *Clim. Dyn.* **35** 1439–59

Fuss S *et al* 2018 Negative emissions—Part 2: costs, potentials and side effects *Environ. Res. Lett.* **13** 063002

Gattuso J-P and Hansson L 2011 *Ocean Acidification* (Oxford: Oxford University Press)

Goodwin P, Williams R G and Ridgwell A 2015 Sensitivity of climate to cumulative carbon emissions due to compensation of ocean heat and carbon uptake *Nat. Geosci.* **8** 29–34

Griffies S M 1998 The Gent–McWilliams Skew Flux *J. Phys. Oceanogr.* **28** 831–41

Harris I, Jones P D, Osborn T J and Lister D H 2014 Updated high-resolution grids of monthly climatic observations—the CRU TS3.10 Dataset *Int. J. Climatol.* **34** 623–42

Heinze C *et al* 2019 ESD reviews: climate feedbacks in the Earth system and prospects for their evaluation *Earth Syst. Dynamics* **10** 379–452

Heinze C, Maier-Reimer E, Winguth A M E and Archer D 1999 A global oceanic sediment model for long-term climate studies *Global Biogeochem. Cycles* **13** 221–50

IPCC 2013 Summary for Policymakers *Climate Change 2013: The Physical Science Basis. Contribution of Working Group I to the Fifth Assessment Report of the Intergovernmental Panel on Climate Change* (Cambridge: Cambridge University Press) 3–30

IPCC 2018 Summary for Policymakers *Global Warming of 1.5 °C. An IPCC Special Report on the impacts of global warming of 1.5 °C above pre-industrial levels and related global greenhouse gas emission pathways, in the context of strengthening the global response to the threat of climate change* (Geneva: World Meteorological Organization) p 32

Jeltsch-Thömmes A, Battaglia G, Cartapanis O, Jaccard S L and Joos F 2019 Low terrestrial carbon storage at the Last Glacial Maximum: constraints from multi-proxy data *Clim. Past* **15** 849–79

Jones C *et al* 2016 Simulating the Earth system response to negative emissions *Environ. Res. Lett.* **11** 095012

Joos F *et al* 2013 Carbon dioxide and climate impulse response functions for the computation of greenhouse gas metrics: a multi-model analysis *Atmos. Chem. Phys.* **13** 2793–825

Kalnay E *et al* 1996 The NCEP/NCAR 40-year reanalysis project *Bull. Amer. Meteor. Soc.* **77** 437–72

Keller D P et al 2018 The Carbon Dioxide Removal Model Intercomparison Project (CDRMIP): Rationale and experimental protocol for CMIP6 *Geosci. Model Dev.* **11** 1133–60

Keller K M et al 2017 20th century changes in carbon isotopes and water-use efficiency: Tree-ring-based evaluation of the CLM4.5 and LPX-Bern models *Biogeosciences* **14** 2641–73

Li C, Notz D, Tietsche S and Marotzke J 2013 The transient versus the equilibrium response of sea ice to global warming *J. Clim.* **26** 5624–36

Lienert S and Joos F 2018 A Bayesian ensemble data assimilation to constrain model parameters and land-use carbon emissions *Biogeosciences* **15** 2909–30

Lowe J A, Huntingford C, Raper S C B, Jones C D, Liddicoat S K and Gohar L K 2009 How difficult is it to recover from dangerous levels of global warming? *Environ. Res. Lett.* **4** 014012

MacDougall A H 2013 Reversing climate warming by artificial atmospheric carbon-dioxide removal: can a Holocene-like climate be restored? *Geophys. Res. Lett.* **40** 5480–5

MacDougall A H et al 2020 Is there warming in the pipeline? A multi-model analysis of the zero emissions commitment from CO_2 *Biogeosciences* **17** 2987–3016

MacDougall A H and Friedlingstein P 2015 The origin and limits of the near proportionality between climate warming and cumulative CO_2 emissions *J. Clim.* **28** 4217–30

MacDougall A H, Zickfeld K, Knutti R and Matthews H D 2015 Sensitivity of carbon budgets to permafrost carbon feedbacks and non-CO_2 forcings *Environ. Res. Lett.* **11** 019501

Maier-Reimer E and Hasselmann K 1987 Transport and storage of CO_2 in the ocean—an inorganic ocean-circulation carbon cycle model *Clim. Dyn.* **2** 63–90

Mathesius S, Hofmann M, Caldeira K and Schellnhuber H J 2015 Long-term response of oceans to CO2 removal from the atmosphere *Nat. Clim. Change* **5** 1107–13

Matthews H D, Gillett N P, Stott P A and Zickfeld K 2009 The proportionality of global warming to cumulative carbon emissions *Nature* **459** 829–32

McKinley G A, Fay A R, Eddebbar Y A, Gloege L and Lovenduski N S 2020 External forcing explains recent decadal variability of the ocean carbon sink *AGU Adv.* **1** e2019AV000149

Müller S A, Joos F, Edwards N R and Stocker T F 2006 Water mass distribution and ventilation time scales in a cost-efficient, three-dimensional ocean model *J. Clim.* **19** 5479–99

Müller S A, Joos F, Plattner G K, Edwards N R and Stocker T F 2008 Modeled natural and excess radiocarbon: sensitivities to the gas exchange formulation and ocean transport strength *Global Biogeochem. Cycles* **22** GB3011

Najjar R G and Orr J C 1999 Biotic-HOWTO. Internal OCMIP *Tech. rep.* LSCE/ CEA, Saclay Gif-sur-Yvette

Orr J C et al 2005 Anthropogenic ocean acidification over the twenty-first century and its impact on calcifying organisms *Nature* **437** 681–6

Orr J C and Epitalon J M 2015 Improved routines to model the ocean carbonate system: Mocsy 2.0 *Geosci. Model Dev.* **8** 485–99

Parekh P, Joos F and Müller S A 2008 A modeling assessment of the interplay between aeolian iron fluxes and iron-binding ligands in controlling carbon dioxide fluctuations during Antarctic warm events *Paleoceanography* **23** PA4202

Pfister P L and Stocker T F 2016 Earth system commitments due to delayed mitigation *Environ. Res. Lett.* **11** 014010

Plattner G-K et al 2008 Long-Term climate commitments projected with climate–carbon cycle models *J. Clim.* **21** 2721–51

Pörtner H-O, Karl D M, Boyd P W, Cheung W W L, Lluch-Cota S E, Nojiri Y, Schmidt D N and Zavialov P O 2014 Ocean Systems *Climate Change 2014: Impacts, Adaptation, and Vulnerability. Part A: Global and Sectoral Aspects. Contribution of Working Group II to the Fifth Assessment Report of the Intergovernmental Panel on Climate Change* (Cambridge: Cambridge University Press) pp 411–84

Riahi K et al 2017 The Shared Socioeconomic Pathways and their energy, land use and greenhouse gas emissions implications: an overview *Glob. Environ. Change* **42** 153–68

Ritz S, Stocker T F and Joos F 2011 A coupled dynamical ocean-energy balance atmosphere model for paleoclimate studies *J. Clim.* **24** 349–75

Rogelj J, Forster P M, Kriegler E, Smith C J and Séférian R 2019 Estimating and tracking the remaining carbon budget for stringent climate targets *Nature* **571** 335–42

Roth R, Ritz S P and Joos F 2014 Burial-nutrient feedbacks amplify the sensitivity of atmospheric carbon dioxide to changes in organic matter remineralisation *Earth Syst. Dyn.* **5** 321–43

Samanta A, Anderson B T, Ganguly S, Knyazikhin Y, Nemani R R and Myneni R B 2010 Physical Climate Response to a Reduction of Anthropogenic Climate Forcing *Earth Interact.* **14** 1–11

Schimel D, Grubb M, Joos F, Kaufmann R K, Moos R, Ogana W, Richels R and Wigley T 1997 Stabilisation of atmospheric greenhouse gases: physical, biological, and socio-economic implications in *Intergovernmental Panel on Climate Change Technical Paper III* Houghton J T et al (Geneva: Intergovernmental Panel on Climate Change) p 53

Sherwood S et al 2020 An assessment of Earth's climate sensitivity using multiple lines of evidence *Rev. Geophys.* **58** e2019RG000678

Siegenthaler U and Oeschger H 1978 Predicting future atmospheric carbon dioxide levels *Science* **199** 388–95

Sitch S et al 2003 Evaluation of ecosystem dynamics, plant geography and terrestrial carbon cycling in the LPJ dynamic global vegetation model *Global Change Biol.* **9** 161–85

Smith P et al 2016 Biophysical and economic limits to negative CO_2 emissions *Nature Clim. Change* **6** 42–50

Steinacher M and Joos F 2016 Transient Earth system responses to cumulative carbon dioxide emissions: linearities, uncertainties and probabilities in an observation-constrained model ensemble *Biogeosciences* **13** 1071–103

Steinacher M, Joos F and Stocker T F 2013 Allowable carbon emissions lowered by multiple climate targets *Nature* **499** 197–201

Stocker B D, Roth R, Joos F, Spahni R, Steinacher M, Zaehle S, Bouwman L, Xu R and Prentice IC 2013a Multiple greenhouse-gas feedbacks from the land biosphere under future climate change scenarios *Nat. Clim. Change* **3** 666–72

Stocker T F 2000 Past and future reorganizations in the climate system *Quat. Sci. Rev.* **19** 301–19

Stocker T F et al 2013b Technical summary *Climate Change 2013: The Physical Science Basis. Contribution of Working Group I to the Fifth Assessment Report of the Intergovernmental Panel on Climate Change* (Cambridge: Cambridge University Press)

Stocker T F 2013 The closing door of climate targets *Science* **339** 280–2

Stocker T F and Schmittner A 1997 Influence of CO_2 emission rates on the stability of the thermohaline circulation *Nature* **388** 862–5

Tokarska K B, Stolpe M B, Sippel S, Fischer E M, Smith C J, Lehner F and Knutti R 2020 Past warming trend constrains future warming in CMIP6 models *Sci. Adv.* **6** eaaz9549

Tokarska K B and Zickfeld K 2015 The effectiveness of net negative carbon dioxide emissions in reversing anthropogenic climate change *Environ. Res. Lett.* **10** 094013

Tokarska K B, Zickfeld K and Rogelj J 2019 Path independence of carbon budgets when meeting a stringent global mean

temperature target after an overshoot *Earth's Future* **7** 1283–95

Tschumi T, Joos F, Gehlen M and Heinze C 2011 Deep ocean ventilation, carbon isotopes, marine sedimentation and the deglacial CO_2 rise *Clim. Past* **7** 771–800

Wanninkhof R 2014 Relationship between wind speed and gas exchange over the ocean revisited *Limnol. Oceanography: Methods* **12** 351–62

Williams R G, Goodwin P, Roussenov V M and Bopp L 2016 A framework to understand the transient climate response to emissions *Environ. Res. Lett.* **11** 015003

Zickfeld K, Eby M, Matthews H D and Weaver A J 2009 Setting cumulative emissions targets to reduce the risk of dangerous climate change *Proc. Natl Acad. Sci.* **106** 16 129–16 134

Zickfeld K, MacDougall A H and Matthews H D 2016 On the proportionality between global temperature change and cumulative CO_2 emissions during periods of net negative CO_2 emissions *Environ. Res. Lett.* **11** 055006